












Large-scale topological disruption of chromosome territories 9 and 22 is associated with nonresponse to treatment in CML

Eunice Fabian-Morales^{1,2,3,4}  | David Vallejo-Escamilla^{2,3,4} | Adriana Gudiño^{2,3}  | Alfredo Rodríguez^{4,5}  | Rodrigo González-Barrios^{3,4}  | Yameli L. Rodríguez Torres^{2,3}  | Clementina Castro Hernández^{3,4}  | Alfredo H. de la Torre-Luján⁶ | Diego A. Oliva-Rico^{2,3,4}  | Erandhi C. Ornelas Guzmán^{2,3}  | Alejandro López Saavedra^{2,3,4}  | Sara Frias^{4,7}  | Luis A. Herrera^{3,4,8} 

¹Doctorado en Ciencias Biomédicas, Universidad Nacional Autónoma de México (UNAM), Mexico City, Mexico

²Unidad de Aplicaciones Avanzadas en Microscopía (ADMIRA), Instituto Nacional de Cancerología (INCan), Red de Apoyo a la Investigación (RAI), Universidad Nacional Autónoma de México (UNAM), Mexico City, Mexico

³Unidad de Investigación Biomédica en Cáncer, Instituto Nacional de Cancerología (INCan), Mexico City, Mexico

⁴Departamento de Medicina Genómica y Toxicología Ambiental, Instituto de Investigaciones Biomédicas, Universidad Nacional Autónoma de México, Ciudad Universitaria, Apartado Postal 70228, Mexico City, Mexico

⁵Instituto Nacional de Pediatría (INP), Mexico City, Mexico

⁶Departamento de Hematología, Instituto Nacional de Cancerología (INCan), Mexico City, Mexico

⁷Laboratorio de Citogenética, Instituto Nacional de Pediatría (INP), Mexico City, Mexico

⁸Instituto Nacional de Medicina Genómica (INMEGEN), Mexico City, Mexico

Correspondence

Luis A. Herrera, Dirección General, Instituto Nacional de Medicina Genómica (INMEGEN), Mexico City 14610, Mexico.
Email: lherrera@inmegen.gob.mx

Funding information

This work was partially supported by the Programa de Apoyo a Proyectos de Investigación e Innovación Tecnológica (PAPIIT IN), Universidad Nacional Autónoma de México (UNAM) Grant Number IN208815, with additional support from Consejo Nacional de Ciencia y Tecnología (CONACYT) and Sectorial funds from Instituto Nacional de Cancerología (INCan) and Instituto de Investigaciones Biomédicas (IIB), UNAM, Mexico. Eunice Fabian-Morales was a fellow of the Programa de Doctorado en Ciencias

Abstract

Chronic myeloid leukemia (CML) is a myeloproliferative neoplasm defined by the presence of t(9;22) translocation whose origin has been associated with the tridimensional genome organization. This rearrangement leads to the fusion of *BCR* and *ABL1* genes giving rise to a chimeric protein with constitutive kinase activity. Imatinib, a tyrosine kinase inhibitor (TKI), is used as a first-line treatment for CML, though ~40% of CML patients do not respond. Here, using structured illumination microscopy (SIM) and 3D reconstruction, we studied the 3D organization patterns of the *ABL1* and *BCR* genes, and their chromosome territories (CTs) CT9 and CT22, in CD34+ cells from CML patients that responded or not to TKI. We found that TKI resistance in CML is associated with high levels of structural disruption of CT9 and CT22 in CD34+ cells, increased CT volumes (especially for CT22), intermingling between CT9

Abbreviations: 3C, chromosome conformation capture; 3D, three-dimensional; BM, bone marrow; CML, chronic myeloid leukemia; CTs, chromosome territories; FISH, fluorescence in situ hybridization; HSC, hematopoietic stem cell; LAD, lamina-associated domains; MPB, mobilized peripheral blood; Non-R, nonresponders; Ph, Philadelphia chromosome; PTMs, posttranslational modifications; R, responders; SIM, structured illumination microscopy; TAD, topologically associating domains; TK, tyrosine kinase; TKI, tyrosine kinase inhibitor; WCP, whole chromosome painting.

This is an open access article under the terms of the Creative Commons Attribution-NonCommercial-NoDerivs License, which permits use and distribution in any medium, provided the original work is properly cited, the use is non-commercial and no modifications or adaptations are made.

© 2021 The Authors. *International Journal of Cancer* published by John Wiley & Sons Ltd on behalf of UICC.

Biomédicas, UNAM, Mexico City, Mexico.
 EFM was supported by CONACYT fellowship
 number 281183, CVU 488227.

and CT22, and an open-chromatin epigenetic mark in CT22. Altogether our results suggest that large-scale disruption of CT9 and CT22 correlates with the clinical response of CML patients, which could be translated into a potential prognostic marker of response to treatment in this disease and provide novel insights into the mechanisms underlying resistance to TKI in CML.

KEYWORDS

chromosome territories, chronic myeloid leukemia, genome reorganization, genome topology, leukemia stem cells

What's new?

The t(9;22) translocation and resulting encoding of a chimeric protein with constitutive tyrosine kinase activity is a hallmark of chronic myeloid leukaemia (CML). The genesis of this rearrangement is related to the topological organization of chromatin in the nucleus. Using super-resolution microscopy, the authors studied the topological features of bone marrow stem cells from CML patients. They found that disruption of chromosome territories 9 and 22 associates with non-response to tyrosine kinase inhibitors in CML. The results suggest a novel prognostic marker and provide new insights into the mechanisms underlying treatment resistance in CML and regulation of the 3D genome organization.

1 | INTRODUCTION

The three-dimensional (3D) folding of the genome in the nucleus is a highly organized process associated with gene regulation and cell function in physiology and disease. Fundamental features of genome organization have been revealed by chromosome conformation capture (3C) methods, which have allowed the identification of chromatin contacts.¹ These contact domains are referred to as topologically associating domains (TADs), defined by their preferential internal chromatin interaction with each other rather than with their surrounding sequences.^{2,3} TADs arrange and coalesce within higher-order structures, known as compartments, which have particular interactional and epigenetic states.⁴ A higher level of genome organization in the interphase nucleus comprises chromosome territories (CTs). The DNA of each chromosome is part of an interphase CT; thus, it occupies a region and volume within the 3D nuclear space.^{5,6} The positioning and organization of each CT are not random and appear to be tissue- and cell-type specific, which entails distinct patterns of global genome organization and chromatin-chromatin interactions that diverge with the increasing separation and maturation of cell lineages.^{7,8}

The spatial organization of each CT in the 3D nuclear space widely correlates with chromatin regulation and is therefore intimately linked to epigenetic elements, such as histone posttranslational modifications (PTMs). This organization influences critical processes, such as gene expression, DNA replication and DNA repair.^{3,9} Studying these properties is essential to determine the relation between chromatin structure, its function and its relevance in the maintenance of genomic integrity.

A clear example of the relevance that chromatin structure and CT organization have in the preservation of genomic stability is the

formation of chromosomal translocations, such as t(9;22), which provides a selective advantage in hematopoietic cells, promoting cancer. The physical proximity that two chromosomes have in the interphase nucleus affects the probability of a translocation between them.¹⁰⁻¹² In addition, the translocation frequency has been shown to be positively correlated with the degree of intermingling between adjacent chromosomes,¹³ and with the proximity between chromosome breaks.¹¹

The t(9;22) translocation fuses the *ABL1* and *BCR* genes and originates the “Philadelphia chromosome (Ph)”. The *ABL1* and *BCR* loci and their corresponding CT9 and CT22, respectively, have been described in spatial proximity in hematopoietic cells and have been proposed as crucial factors in the genesis of the t(9;22) translocation.^{14,15} This sole chromosome aberration has a critical role in the pathogenesis of chronic myeloid leukemia (CML) since the *BCR-ABL1* fusion gene encodes a chimeric protein with constitutive tyrosine kinase (TK) activity, which drives the leukemic transformation of a hematopoietic stem cell, producing many cells with the t(9;22) in the chronic phase of the disease. This phenomenon results in an accelerated phase and genetically unstable myeloid cells and finally disease progression.¹⁶

Imatinib mesylate, a potent competitive TK inhibitor (TKI), impedes the interaction of the ATP molecule with the *BCR-ABL1* chimeric protein and thereby inhibits its ability to phosphorylate and activate its downstream target proteins. Currently, imatinib is the first-line treatment for all newly diagnosed CML patients and has improved the prognosis of patients in the chronic phase of the disease.¹⁷ However, approximately 40% of patients do not respond to first-line TKI treatment due to toxicity or lack of efficacy.¹⁸ For patients failing the TKI first-line treatment, a treatment change is mandatory to limit the risk of progression and death. CML is a paradigmatic model for analysis since a single chromosome aberration

produces the leukemic phenotype, and its etiology is associated with the organization of the genome.

Three-dimensional fluorescent in situ hybridization (3D-FISH), high-resolution imaging technologies, such as 3D structured illumination microscopy (3D-SIM), and image reconstruction have proven to be powerful and efficient tools for analyzing the topological organization of chromatin within the nucleus.^{19,20} In the present work, we explored the topological features and histone PTMs of CT9 and CT22, as well as of the *BCR* and *ABL1* genes involved in the t(9;22) translocation using 3D-FISH and 3D-SIM technologies with CD34⁺ cells from CML patients. We studied bone marrow (BM) CD34⁺ cells from patients with CML at the time of diagnosis and from patients with TKI treatment. These patients were further subdivided into responders and nonresponders based on their clinical response to TKI first-line treatment. Striking differences in the topological organization and histone PTMs of CT9 and CT22 were observed between the responder and nonresponder groups. The most relevant and evident topological difference was the consistently high levels of structural disruption of CT9 and CT22 observed in CD34⁺ cells from patients who did not respond to TKI treatment. Our findings highlight an intrinsic association between the 3D organization of the genome and the potential clinical outcome of TKI treatment for CML, suggesting that CT rearrangements have the potential to change the inheritance system of a cell and are associated with drug resistance.

2 | MATERIALS AND METHODS

2.1 | Patients sample collection

Remnant BM samples from CML patients in clinical follow-up were used in our study (age range 23-64 years old; median = 37 years old). CML patients at the moment of diagnosis (naïve) were subclassified as responders (R) or nonresponders (non-R) based on their response to tyrosine kinase inhibitor (TKI) first-line treatment with imatinib using hematological, molecular and cytogenetic response criteria.²¹ Using the same parameters, CML patients receiving TKI treatment were subclassified into the R and non-R groups. Healthy controls included 2 BM samples from healthy donors, one of which was purchased from Lonza (1M-105, Lonza), and MPB from five healthy donors obtained at INCan. Details on the patients and healthy donors are described in Table S1.

Patient BM was cytogenetically screened, and only patients with the presence of the Philadelphia chromosome (Ph⁺) and no additional chromosome aberrations were included in our study (Figure S1). Patients previously treated with hydroxyurea for more than 6 months and TKI first-line treatment (imatinib) for more than 3 months were excluded. Likewise, patients with first-line treatment other than imatinib or with comorbidities were also excluded.

2.2 | Definition of response criteria

The response criteria to imatinib used in our study have been previously defined (see Supporting Information Methods for further details).^{22,23}

Only patients with optimal hematological, molecular and cytogenetic responses with a minimal follow-up of 12 months were considered responders. Patients with a suboptimal and resistant response after 12 months of follow-up were considered nonresponders.

2.3 | Karyotype analysis

Karyotype analysis was performed in all samples included in our study. Chromosome preparation and karyotyping were performed according to standard methods and described according to the International System for Human Cytogenomic Nomenclature 2020 guidelines.²⁴

As part of the inclusion criteria, only samples with normal karyotypes were included in the healthy BM population, MPB and TKI responders. As part of the inclusion criteria for naïve patients, detection of t(9;22) was required. However, given that the TKI non-R group does not obtain a complete cytogenetic response, the cells of these patients showed mosaicism, and we could observe karyotypes with and without t(9;22). None of the included patients showed additional chromosome abnormalities apart from t(9;22) (Figure S1).

2.4 | Isolation of CD34⁺ cells

In CML, the long-term hematopoietic stem cell (HSC) containing the t(9;22) translocation has been established as the cell of origin by *in vivo* clonality studies in humans.^{25,26} The CD34 antigen is the most important marker for human HSCs and was used in this work for their isolation.

CD34⁺ hematopoietic stem and progenitor cells were isolated from BM and MPB. First, fresh mononuclear cells were isolated using Ficoll-Hypaque (Sigma-Aldrich) density gradient centrifugation. Subsequently, CD34⁺ cells were purified from the mononuclear fraction through positive selection using anti-CD34-coated microbeads and Midi-Macs separation columns (Miltenyi, Biotec, Bergisch Gladbach, Germany) according to the manufacturer's instructions.

2.5 | Three-dimensional fluorescence in situ hybridization

FISH was performed on human CD34⁺ cells from BM and MPB adhered to poly-L-lysine-coated slides, as previously described with some modifications²⁷ (see details in Supporting Information Methods). For hybridization, a *BCR/ABL1* dual color dual fusion probe (Ref.30-191032 Abbott Molecular, Vysis, Abbott Park, IL) and whole chromosome paint probes for CT9 and 22 (Ref.D-1112-125-IR; D1113-125-IR, MetaSystems, North Royalton, OH) were used.

2.6 | Conventional FISH

The hybridization pattern of the probes used in our study was verified by conventional FISH on metaphase spreads. The FISH technique was

performed according to the manufacturer's instructions (Vysis and MethaSystems Company). Representative images of the whole chromosome painting (WCP) for chromosomes 9 and 22 on metaphase spreads are shown in Figure S2.

2.7 | 3D immuno-FISH

Immuno-FISH was performed as previously described with some modifications (see Supporting Information Methods for details).²⁸ The cells were incubated with the primary antibodies H3K9ac (Abcam Cat. No. ab10812) and H3K27me3 (Abcam Cat. No. ab6002); and the secondary antibodies ATTO 647 N (goat anti-rabbit, active motif cat. no. 15048) and DyLight 405 (goat anti-mouse, Thermo Fisher cat. no. 35501BID) were used. For FISH hybridization painting probes for chromosomes 9 and 22 (Ref.D-1112-125-IR; D1113-125-IR, MetaSystems) were used.

2.8 | Microscopy and image acquisition

The detailed specifications of the equipment used, and the 3D SIM imaging capture procedures are described in Supporting Information Methods.

2.9 | Image analysis and CT compartment definition

Three-dimensional image reconstruction and analysis were performed with Imaris software (Version 9.1.2, Bitplane). The full 3D image was used for analysis, and a minimum of 25 cells per subject were studied. The number of cells analyzed was determined taking into consideration a standard protocol for SIM;²⁹ standard cytogenetic protocols also establish that the analysis of 25 cells is enough to identify alterations present in at least 12% of the cell population with 95% confidence. In addition, CML BM is considered to be tissue with a highly homogeneous karyotype, and only patients with the Philadelphia chromosome in every analyzed cell were included.³⁰ The workflow for image analysis, as well as the 3D reconstruction and the consequent definition of the CTs compartments, are detailed described in Supporting Information Methods.

2.10 | Definition and analysis of nuclear topological features

Volumes of CTs and intermingling between heterologous chromosomes were calculated. Likewise, chromatin decompaction factor, histone PTM occupancy on CTs, minimum distances between genes and CTs, and their nuclear relative radial position, as well as gene location within CTs were also evaluated. The definition and

analysis of each feature are described in Supporting Information Methods.

2.11 | Statistical analyses

Statistical analysis was performed using the Kruskal-Wallis test. A *P* value of .01 to .05 was considered significant (*), *P* values of .001 to .01 were considered very significant (**), and *P* values <.001 were considered extremely significant (***, ****). Data were analyzed with GraphPad Prism 7.0 software.

3 | RESULTS

3.1 | CT9 and CT22 are highly disrupted in CD34+ cells from CML patients who did not respond to TKI treatment

We used 3D-SIM technology for the analysis of CT9 and CT22 in CD34+ cells isolated from bone marrow (BM) (*n* = 2) or mobilized peripheral blood (MPB) (*n* = 5) from healthy donors or CML patients who were naïve to treatment (*n* = 10) and treated with TKIs (*n* = 10). CML patients were subclassified based on their response or nonresponse to TKI first-line treatment (Imatinib), leading to four groups of CML patients: (a) naïve patients who responded to TKI after being treated (naïve R); (b) naïve patients who did not respond to their further TKI treatment (naïve non-R); (c) patients who received TKI and responded (TKI-R); and (d) patients who received TKI and did not respond (TKI non-R; Figure 1A). The response criteria used in our study were defined according to the NCCN Clinical Practice Guidelines in Oncology for CML.²¹ Hematological, molecular and cytogenetic responses were evaluated. Details on demographics and disease characteristics for all patients are summarized in Table S1. Samples were processed for 3D-FISH, and 3D reconstruction was performed using SIM images. For every acquired CD34+ cell, a 3D-FISH reconstruction was made for the *ABL1* and *BCR* genes on the *x,y* and *x,z* axes (Figure 1B), as well as a 3D-FISH reconstruction for the chromosome painting of CT9 and CT22 on the *x,y* and *x,z* axes (Figure 1C). Locus-specific 3D-FISH for *BCR* and *ABL1* showed the expected t(9;22) translocation in the naïve CML patients as well as in the TKI non-R CML patients (Figure 1D).

After analyzing the 3D reconstructions for CT9 and CT22, we observed a differential amount of chromatin compartments per CT (Figure 1E); in particular, the non-R patients showed a pattern of CT compartmentalization that was apparently disrupted compared to the healthy controls. Interestingly, disruption was not observed in metaphase chromosomes from CML patients (Figure S1), indicating that the topological rearrangements appear exclusively during the interphase.

When we quantified the number of compartments per CT, we found that they substantially varied among the groups and that they

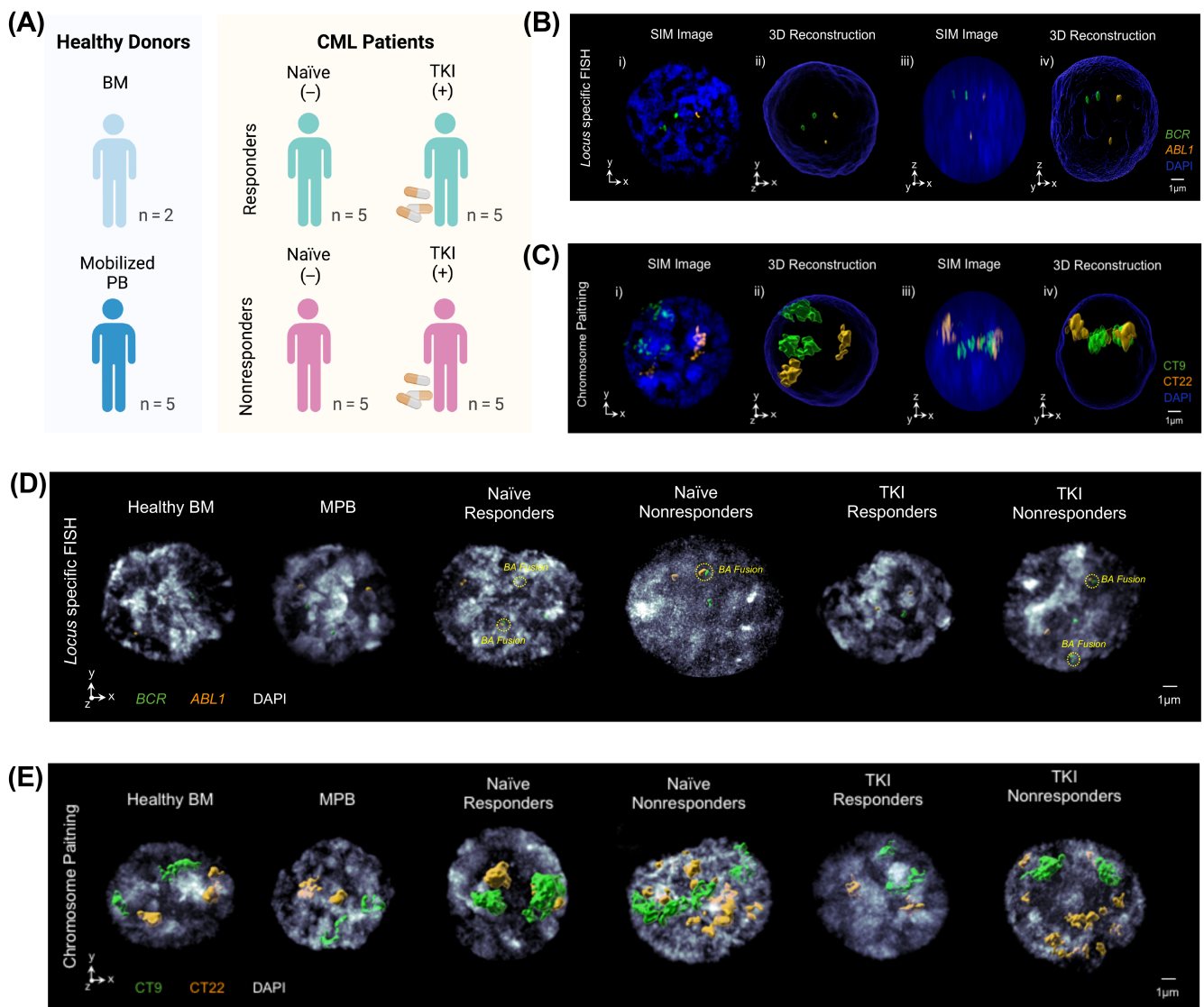


FIGURE 1 Three-dimensional structured illumination microscopy (3D-SIM) for the study of chromosome territories in CML. (A) Patients were invited to participate in our study at the time of diagnosis (naïve) and classified as responders (R) or nonresponders (non-R) based on their further response to TKI first-line treatment. Another subset of patients was studied after TKI treatment and classified as R and non-R (Table S1). The analyzed CD34+ cells were isolated from bone marrow (BM) samples of the CML patients. Likewise, BM samples and mobilized peripheral blood (MPB) from healthy donors were used as controls. (B) Three-dimensional-FISH for the *BCR* (green signal) and *ABL1* (orange signal) genes. The image shows a representative mid-cross-section (x,y axes) from 3D SIM capture (i) and its respective 3D reconstruction (ii) of CD34+ cells from a healthy donor. Orthogonal cross-section through the entire 3D image stack (x,z axes) (iii) and its 3D reconstruction (iv) of the same cell is shown. Note that only three out of the four loci expected in a healthy cell are visible in (i), and since the fourth signal is localized in another plane it is only observed in the 3D reconstruction (ii), and x,z axial view (iii and iv). Nuclei are counterstained with DAPI (blue). (C) Three-dimensional FISH for chromosome territories (CT) 9 and 22. A representative mid-cross-section (x,y axes) from a 3D SIM image (i) and its respective 3D reconstruction (ii) of a healthy interphase CD34+ nucleus, showing CT9 (green) and CT22 (orange). Orthogonal cross-section through the entire 3D image stack (x,z axes) from the same cell nucleus (iii) and its respective 3D reconstruction (iv). Nuclei were counterstained with DAPI (blue). (D) Representative SIM and 3D reconstruction of CD34+ cells from locus-specific 3D-FISH for the *BCR* (green) and *ABL1* (orange) genes. Note that translocation $t(9;22)$, which fuses the *BCR* and *ABL1* genes, is present in cells from naïve and TKI non-R CML patients (dotted circles). Nuclei are counterstained with DAPI (white). (E) Representative SIM and 3D reconstruction of CD34+ cells from 3D-FISH chromosome paintings are shown for CT9 (green) and CT22 (orange). Note that CTs appear disrupted in the naïve non-R and TKI non-R groups, in sharp contrast to the CD34+ cells from healthy donors and the naïve-R and TKI-R groups. Nuclei are counterstained with DAPI (white). Scale bars represent 1 μm . See also Figure S1 [Color figure can be viewed at wileyonlinelibrary.com]

felt into distinct patterns that we called “CT variants.” In this regard, a CT was considered “disrupted” when it was compartmentalized in more than five compartments. Hence, a total of 14 distinct CT

variants were distinguished, spanning at least two categories: non-disrupted CTs (variants 1-10) and disrupted CTs (variants 11-14; Figure 2A). The most common pattern in the healthy groups and in

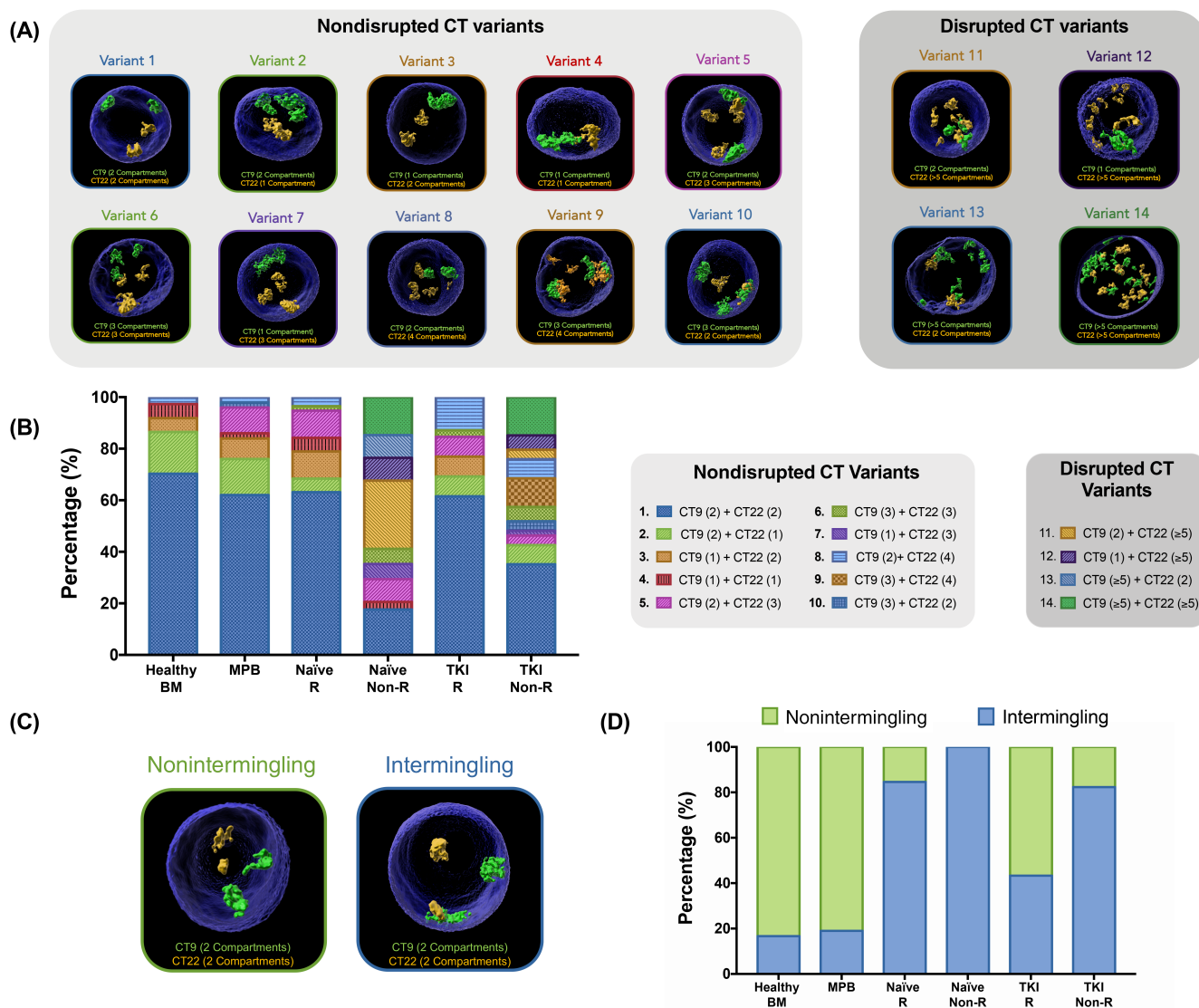


FIGURE 2 CT disruption correlates with the absence of a response to TKIs. (A) Representative 3D reconstructions showing the different CT variants identified in CD34+ cells. CT variants were numbered from 1 to 14 according to the different combinations of identified CT compartments. Cells were classified according to the number of identified compartments in “Non-Disrupted CT” (Variants 1-10) or “Disrupted CT” (Variants 11-14) when 5 or more compartments of CT9 and/or CT22 were identified. The total number of compartments per CT is indicated in parentheses. (B) Distribution of the CT variants per group. Note that the non-R groups have a large proportion of disrupted CT variants. (C) Left: Representative 3D reconstruction showing a cell with completely separated heterologous CT compartments (nonintermingling). Right: Representative 3D reconstruction showing a cell with an overlap between heterologous CTs (intermingling). (D) Proportion of intermingling between the heterologous CTs in each group. The largest proportion of cells with intermingling appeared in the groups with the t(9;22) translocation. Data in B and D are presented as stacked bars [Color figure can be viewed at wileyonlinelibrary.com]

the responder CML patients was CT variant 1, characterized by the presence of two compartments for both CT9 and CT22. Variants 2, 3 and 4 were common in healthy samples and were characterized by coalescence of CT9 or CT22 into a single compartment without distinguishable separation. Variants 5-10 (except variant 7) showed CT9 or CT22 with two or more compartments but never more than four compartments. In stark contrast, CTs in the CML nonresponder patients exhibited a higher variability of CT variants and strikingly showed a high proportion of disrupted variants (variants 11-14; Figure 2B). This variability in CT9 and CT22 organization is an indicative of

heterogeneity at the single-cell level, possibly explained by the intrinsic variation of CD34+ cell subpopulations, but also a reflection of the functional changes in the interphase genome architecture related to the control of gene expression. In turn, the CTs disruption reveals how the mechanisms maintaining chromatin structure are dysregulated in CML.

Additionally, we quantified the number of cells with intermingling regions between heterologous CTs, regardless of the number of identified compartments (Figure 2C). As expected, the groups with t(9;22) translocation showed a high percentage of intermingling between

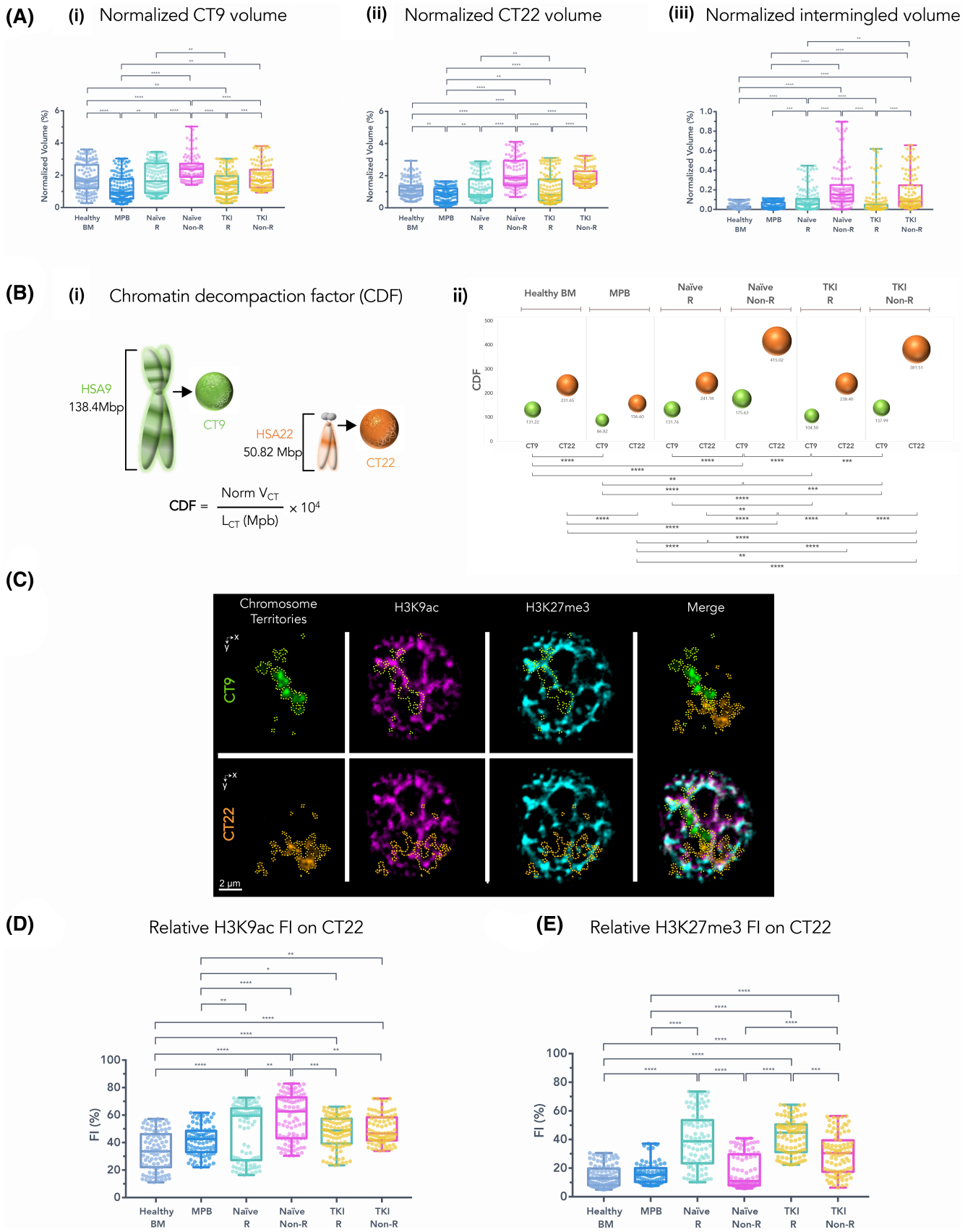


FIGURE 3 Legend on next page.

their CTs, particularly in the non-R groups, in comparison to the groups without the chromosomal translocation (Figure 2D). Of note, the percentage of cells with intermingling CTs was higher in the TKI-R patients than in the healthy controls, despite the absence of the t(9;22) translocation. Given the association between CT spatial proximity and the increasing probability of engaging in translocation, the elevated proportion of intermingled CTs in the TKI-R group suggests a topological feature that may predispose patients to t(9;22) formation.

3.2 | CT disruption is associated with increased CT volumes, extensive regions of intermingling and increased chromatin decompaction

Given the levels of CT disruption in the TKI non-R groups, we decided to explore whether these changes were reflected in the volumes of CT9 and CT22. To avoid artifacts derived from the variable nuclear sizes, we normalized the CT volumes in reference to their respective nuclei (Figure S3Ai,ii). After calculating the nuclear volumes of the CD34+ cells from all groups, we observed the largest nuclei in the naïve non-R group and the smallest nuclei in the MPB group (Figure S3B). After CT normalization, we observed clear differences among CML patients; in particular, the non-R populations showed the highest volumes for CT9 (Figure 3A-i) and CT22 (Figure 3A-ii).

The volume of the intermingling regions between heterologous CTs was also calculated (Figure S3Aiii), and the naïve non-R group showed the highest intermingling volume (Figure 3A-iii). Interestingly, in some cells of the TKI-R group, the intermingling volume was similar to the volumes observed in the CML patients with t(9;22).

To evaluate CTs overlap, we calculated the proportion of the intermingling region for each CT (Figure S3Aiv). We determined the percentage of CT9 overlapping with CT22 (Figure S3C) and the percentage of CT22 overlapping with CT9 (Figure S3D). As we observed in the intermingling analysis, the highest overlapping proportion for both CT9 and CT22 occurred in the naïve non-R group, followed by

the naïve-R group, and both CTs showed similar overlapping percentages.

Using the chromatin decompaction factor (CDF), defined as the normalized volume of 1 mega-base pair (Mbp) of the DNA sequence³¹ (Figure 3B-i), we found that CT22 was more decompacted than CT9 in all groups, and the maximum CDF for both CT9 and CT22 was observed in the naïve non-R and TKI non-R populations (Figure 3B-ii). CDF analysis of the total nuclear volume showed that MPB was the group with the smallest decompaction, whereas naïve non-R cells were more decompacted than naïve-R cells (Figure S3E). These results suggest that the CT disruption observed in the non-R patient groups associated with an increase in chromosome volume and a high degree of chromatin decompaction, particularly in CT22.

3.3 | Histone PTMs are differentially distributed in the CTs and in the nucleus of naïve-R and naïve non-R populations

Histone PTMs are preponderant in the different states of compaction and activation of chromatin, which ultimately determine the formation of TADs and CT compartments. Given the differences in CTs decompaction observed among the CML groups, we decided to evaluate whether histone PTMs are associated with these changes. Therefore, by using 3D immuno-FISH, we measured the presence of H3K9ac and H3K27me3, which are considered open and closed chromatin marks respectively,^{32,33} on CT9, CT22 and the whole nucleus (Figure 3C and Figure S4A).

For the naïve non-R group, we observed that CT22 displayed high levels of H3K9ac (Figure 3D) and reduced levels of H3K27me3 (Figure 3E). Interestingly, the histone occupancy analysis of CT9 showed the opposite result: the percentage of H3K9ac occupancy on CT9 was significantly low (Figure S3F), and H3K27me3 was increased in the naïve non-R group (Figure S3G). Likewise, we further analyzed the presence of these histone marks within the whole nucleus of

FIGURE 3 The volumes and chromatin decompaction factors of CT9 and CT22 were significantly increased in nonresponding CML. (A) Normalized volumes for CTs and intermingling regions. (i) Comparison of the normalized CT9 volumes among groups. (ii) Comparison of the normalized CT22 volumes among groups. (iii) Normalized intermingling volume between CT9 and CT22 among groups. Note that the volumes for CT9 and CT22 and the intermingling volumes were significantly higher in the non-R groups. See Figure S3 for an explanation of how normalizations were performed. (B) Chromatin decompaction factor (CDF). (i) Schematic representation of CDF obtention. CDF measurement considers the normalized CT volume ($\text{Norm } V_{CT}$) and chromosome length (L_{CT}). For representative purposes, human chromosomes 9 (HSA9) and 22 (HSA22) are shown in their mitotic and predicted interphase decompacted conformations. (ii) Comparison of the CDF mean among groups. Comparisons were made only among homologous CTs but not among heterologous CTs. The CDFs for CT9 and CT22 were considerably larger in the non-R groups than in the other groups. (C) Representative 3D-SIM images of CD34+ cells from a naïve non-R CML patient showing simultaneous 3D-FISH and immunofluorescence. The images show chromosome painting for CT9 (green) and CT22 (orange) combined with immunofluorescence for the histone marks H3K9ac (magenta) and H3K27me3 (cyan). The edges of each CT are depicted with dotted outlines. Scale bar: 2 μm . (D) Comparison of the relative fluorescence intensity (FI) of H3K9ac on CT22 among groups. Bar charts show the average H3K9ac/CT22 signal ratio. Relative levels of H3K9ac were greater in CT22 of the cells of non-R groups. (E) Comparison of the relative fluorescence intensity (FI) of H3K27me3 on CT22 among groups. Bar charts show the average H3K27me3/CT22 signal ratio. Relative levels of H3K27me3 were smaller in CT22 of the cells of non-R groups cells. Data in graphs A, D and E are represented as boxplots and bubble chart in B. *P* values of .01 to .05 were considered significant (*), *P* values of .001 to .01 were considered very significant (**), and *P* values <.001 were considered extremely significant (***, ****). See also Figure S3 [Color figure can be viewed at wileyonlinelibrary.com]

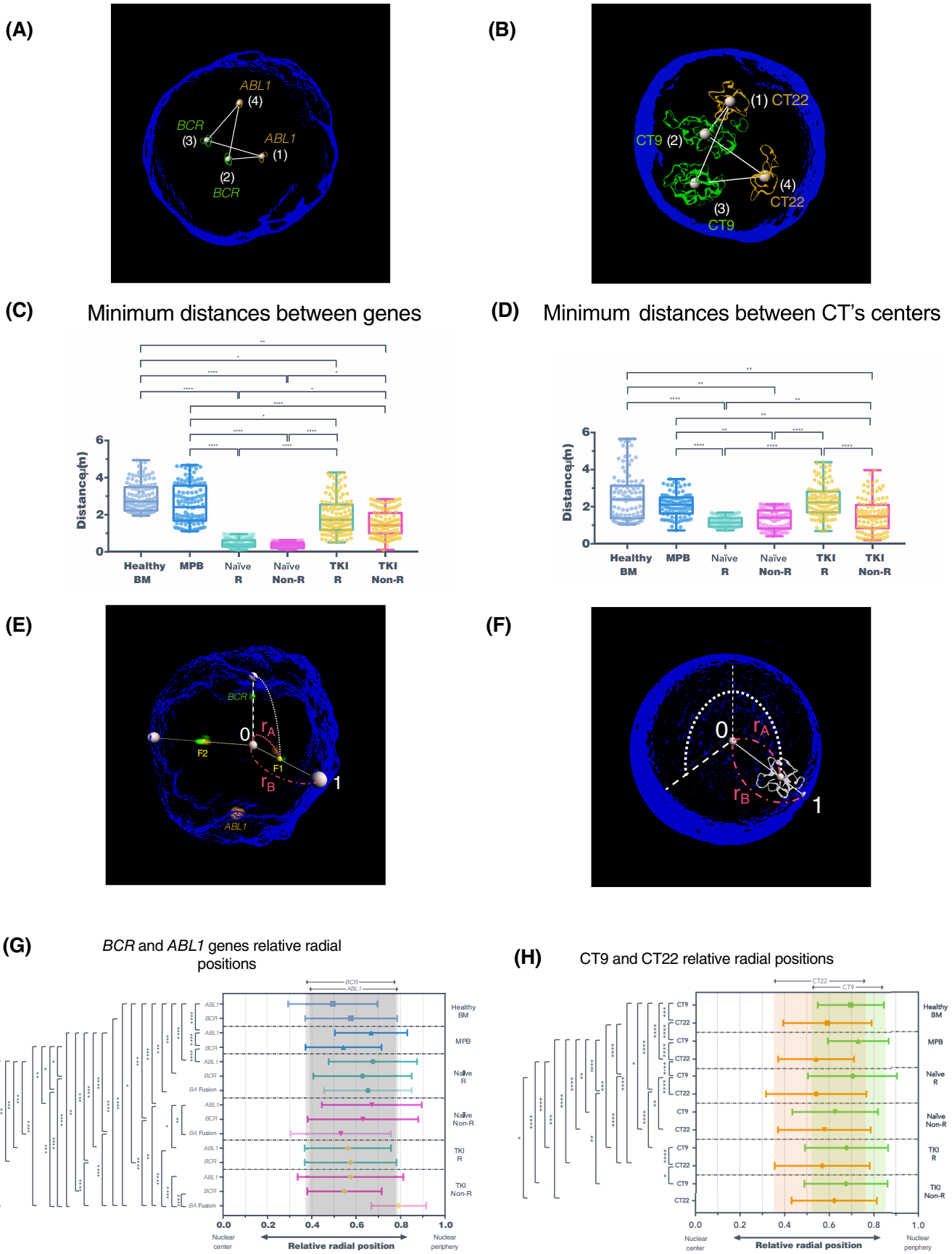


FIGURE 4 Legend on next page.

CD34+ cells, finding the highest levels of H3K9ac and H3K27me3 in the nucleus of TKI non-R and Naïve R groups respectively (Figure S4B,C).

Taken together, we find interesting and worth highlighting the case of CT22 from the Naïve Non-R population, in which the significant increase of the open chromatin mark enrichment, H3K9ac, coincides with its significant increase in volume and CDF compared to the other study groups. This observation is suggestive of a direct association, but given the complexity of chromatin dynamics, complementary analyses are necessary to determine this suggestive association.

Finally, in addition to the evident differences between study groups observed when comparing the enrichment of PTM marks between CTs and nuclei, our data also expose intrinsic differences when comparing these elements within the same population.

3.4 | Minimum distances between CTs correlate with their intermingling

To investigate the correlation between the distance of *BCR* and *ABL1* or the heterologous CTs and their intermingling regions, we measured the minimum distances between the *BCR* and *ABL1* genes, considering the distances between genes forming the *BCR-ABL* fusion (*BA* fusion) in the groups with the presence of *t(9;22)* (Figure 4A), as well as between CT9 and CT22 (Figure 4B). Disrupted CTs were not considered in this analysis since their variability would introduce bias in the analysis. Healthy groups showed the longest minimum distances in both measurements, between genes (Figure 4C) and between heterologous CTs (Figure 4D). Moreover, the shortest minimum distance in both cases was observed in the naïve groups, where the *t(9;22)* translocation was present. These observations support the notion that the

shorter the distance between CTs, the larger their intermingling region is and vice versa. In addition, we observed a significant reduction in the minimum distances between the *BCR* and *ABL1* genes in the TKI-R group but not between CTs compared to those in the healthy controls. These results suggest an increased likelihood of translocation occurrence in the TKI-R group compared to the healthy groups, since heterologous CTs and the *BCR* and *ABL1* genes remain in significant proximity despite the *t(9;22)* translocation no longer being present.

3.5 | The nuclear position of CT9 and CT22 does not change when the *t(9;22)* translocation is present

The relative radial positions of *ABL1*, *BCR* and the *BA* fusion gene (Figure 4E), as well as the relative radial position of each CT (disrupted CTs were not considered; Figure 4F), were analyzed to determine whether the changes in CT volume and compartmentalization would affect the nuclear positioning of the *BCR* and *ABL1* genes as well as their CTs.

When we compared the relative radial positions of *BCR* and *ABL1* per group (Figure 4G), we observed in the MPB group that the *ABL1* gene was positioned significantly more towards the nuclear periphery than *BCR*. In addition, we observed that the *ABL1* gene from the healthy BM and the TKI-R groups was positioned towards the nuclear center compared to that of the MPB, naïve-R and naïve non-R groups. However, the position of the *BCR* alleles showed differences only between the MPB and naïve-R groups and was located more towards the periphery in the last group.

The position of the *BA* fusion was compared among the groups with the *t(9;22)* translocation. Interestingly, the fusion's position differed significantly among all analyzed groups. *BA* fusion was located

FIGURE 4 The presence of the *t(9;22)* translocation does not change the CTs relative radial positions in the nucleus. (A) Minimum distances between the *BCR* and *ABL1* genes. Representative 3D reconstruction showing how the distances between the center of the gene probe signals were obtained. The minimum distance was defined as the shortest distance between the *BCR* and *ABL1* probe signals (numerically marked in the image), in this example, the *ABL1* (1) and *BCR* (2) signals are the closest. (B) Minimum distances between CT9 and CT22. Representative 3D reconstruction showing how the distances between the center of the CTs were obtained. The minimum distance was defined as the shortest distance between heterologous CTs 9 and 22. In the image, each of the CTs is numbered and CT22 (1) and CT9 (2) are exemplified as the closest heterologous CTs. (C) Comparison of the minimum distances between the *BCR* and *ABL1* genes among groups. (D) Comparison of the minimum distances between CT9 and CT22 among groups. (E) Representative 3D reconstruction of a cell with *t(9;22)* showing one signal for the *BCR* gene (green), one signal for the *ABL1* gene (orange) and two fusion signals (F1 and F2). The relative radial position (r) of each allele was calculated. The nucleus center was defined as 0, and the distance between 0 and each allele signal was defined as r_A . The nuclear ratio (r_B) was defined as the distance between 0 and the nuclear periphery (1) passing through the signal center. The relative radial position (r) with respect to the nuclear center was calculated as a fraction of r_B ($r = r_A/r_B$). (F) Representative 3D reconstruction showing how the relative radial position (r) of CTs was calculated. The relative radial position was measured taking into account each CT compartment center. The nucleus center was defined as 0, and the distance between 0 and each CT center signal was defined as r_A . The nuclear ratio (r_B) was defined as the distance between 0 and the nuclear periphery (1) passing through the signal center. The relative radial position (r) with respect to the nuclear center was calculated as a fraction of r_B ($r = r_A/r_B$). (G) Relative radial positions (r) of *BCR* and *ABL1*. Bars represent the position range of *ABL1*, *BCR* and the *BA* fusion genes inside the nucleus. A tendency to 0 indicates proximity to the nuclear center, whereas a tendency to 1 indicates proximity to the periphery. The shaded bars inside the graph cover the dispersion (SD) considering all populations for *ABL1* (light gray) and *BCR* (dark gray) positions. (H) Relative radial positions (r) of CT9 and CT22. Bars represent the position range of CT9 and CT22 inside the nucleus. A tendency to 0 indicates proximity to the nuclear center, whereas a tendency to 1 indicates proximity to the periphery. The shaded bars inside the graph cover the dispersion (SD) considering all populations for CT9 (green) and CT22 (orange). Data in C and D are presented as boxplots and forest plots in G and H. P values of .01 to .05 were considered significant (*), P values of .001 to .01 were considered very significant (**), and P values <.001 were considered extremely significant (***, ****) [Color figure can be viewed at wileyonlinelibrary.com]

more peripherally in the TKI non-R group (Figure 4G), whereas in the naïve non-R group it tended to be located more towards the nuclear center. Since a correlation between the levels of gene expression and the nuclear relative radial position has been identified in several studies, the distinctive position of the BA fusion in the TKI non-R group could indicate such an association.

Comparison of the CTs relative radial position showed that CT9 tended to be located more towards the nuclear periphery than CT22 (Figure 4H). Interestingly, for both CML non-R groups, the CTs appear to approach. In addition, the CT9 position in the naïve non-R group was located significantly more towards the nuclear center than that in the naïve-R group. We did not observe differences between groups regarding the relative radial position of CT22. Of note, the CT position in the groups with t(9;22) did not differ from the CT positions in the healthy BM group.

3.6 | The location of genes with respect to their CTs is different among CML groups

We continue characterizing the topological features of the *BCR* and *ABL1* genes in CML by analyzing their location with respect to their CTs using quadruplex FISH, followed by 3D-SIM reconstruction that was analyzed in the x,y axes (Figure 5A) and the x,z axes (Figure 5B). We discovered several allele location patterns, which were classified according to the location of *ABL1*, *BCR* or the BA fusion gene (inside or outside its respective CT; Supporting Information Methods). Cells with the BA fusion still had one nonfused allele for the *BCR* and *ABL1* genes (Figure 5C, left panel).

In this analysis (Figure 5C, right panel), the most common pattern observed in the healthy BM group was one allele inside and another allele outside of its CT (location pattern A). In contrast, the MPB showed nine different location patterns, probably due to topological changes induced by the mobilization scheme. Interestingly, most combinatorial patterns observed in the CML patients involved the *ABL1* allele outside of CT9. Notably, in the TKI-R group that lost the t(9;22) translocation, only two different location patterns (location patterns D and F) were observed, and none of them was the location pattern most frequently observed in the healthy BM or MPB group. Finally, the TKI non-R group showed the most diverse and heterogeneous array of location patterns.

However, it should be noted that the BA fusion signal was observed within both CT9 and CT22, without significant differences in the frequency observed for each CT ($P > .05$). Altogether, these observations demonstrate a substantial variability in the location of the genes between CML groups and a behavior that diverges from healthy conditions, which may be linked to differences in the transcriptional activity of these genes in every analyzed condition (Figure 5C, right panel).

In order to provide an approach to understand the observed variation in gene position, we explored lamina-associated domains (LADs), since they have been linked to establishing interphase chromosomal topology and transcriptional activity.³⁴ However, after intensively

reviewing the literature, we found published data from the mapping of LADs in human fibroblasts.³⁵ Upon analysis of the NKI LADs (Tig3) track using the UCSC Genome Browser, we confirmed that neither *BCR* nor *ABL1* are located inside a LAD. Moreover, the *BCR* locus is located >15 kb downstream of the nearest reported LAD on chromosome 22, and the *ABL1* locus is >8 Mb away from the closest reported LAD on chromosome 9. If this location has a functional relevance and whether it is preserved in the hematopoietic lineage remains to be experimentally explored.

4 | DISCUSSION

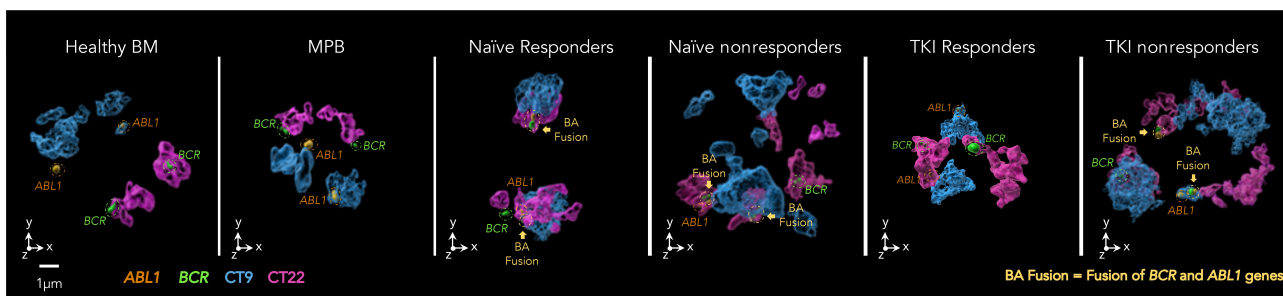
The organization of the genome has a critical role in the regulation of cellular functions. Chromosomes organize a network of genetic interactions involving the entire genome, thus creating an inheritance system with 3D nuclear organization. It is therefore expected that structural alterations of the chromosomes, such as translocations, that reshuffle the genomic topological domains will have important consequences at different levels.³⁶

Here, we used super-resolution microscopy to study the effects of the t(9;22) translocation on the 3D genome architecture of CML cells. Using 3D-SIM, we studied CD34+ cells from the BM of CML patients and discovered that the presence of t(9;22) has a major impact on the chromatin organization of CML cells at distinct levels, including the repositioning of alleles, chromatin decompaction and CT positioning. We discovered a large-scale topological reorganization of the genome, reflected as a major disruption of CT9 and CT22, mainly in nonresponder CML patients (compared to healthy donors and CML patients who responded favorably to imatinib). These observations suggest a direct association between the topological properties of CT9 and CT22 and the response of CML patients to therapy. Of relevance is the observation that disruption of CT9 and CT22 exists at diagnosis in nonresponder CML patients (naïve non-R group), suggesting that nuclear structural features of these patients could prime them to be nonresponsive.

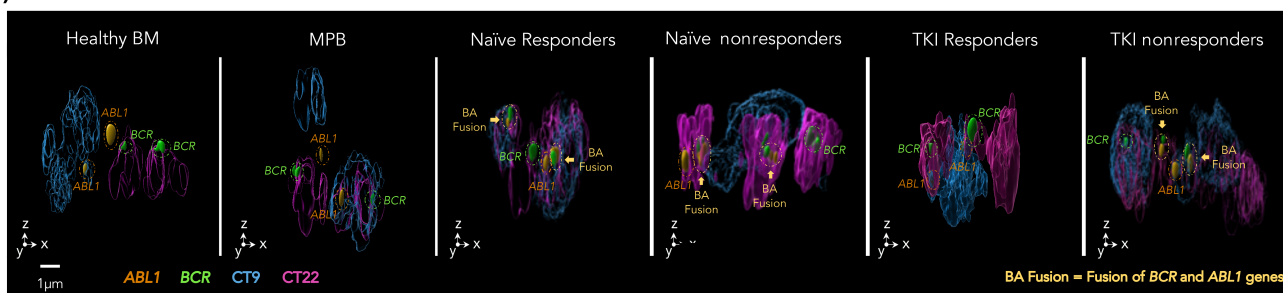
Previous studies in cancer cells using conformational capture of chromosomes (3C) have shown that chromosome structural alterations can lead to TAD fusions, thus forming neo-TADs that reconfigure the regulatory interactions among genomic elements.³⁷ Other research has linked the dynamic formation of chromatin compartments to tamoxifen resistance in breast cancer.³⁸ This evidence reveals an association between genome reorganization and therapy response in cancer patients. Our results expand these previous findings, highlighting the fact that large-scale chromatin reorganization is not only evident at the molecular level but can also be detected using microscopy.

Accordingly, the study of nuclear topology and chromatin conformation is becoming increasingly crucial in understanding carcinogenic processes and resistance to cancer treatments. Our study aimed to explore the potential large-scale topological changes in CML focusing on CT9 and CT22. Consistent with the disruption observed in these CTs, we found a significant increase in the volume, particularly of

(A)



(B)



(C)

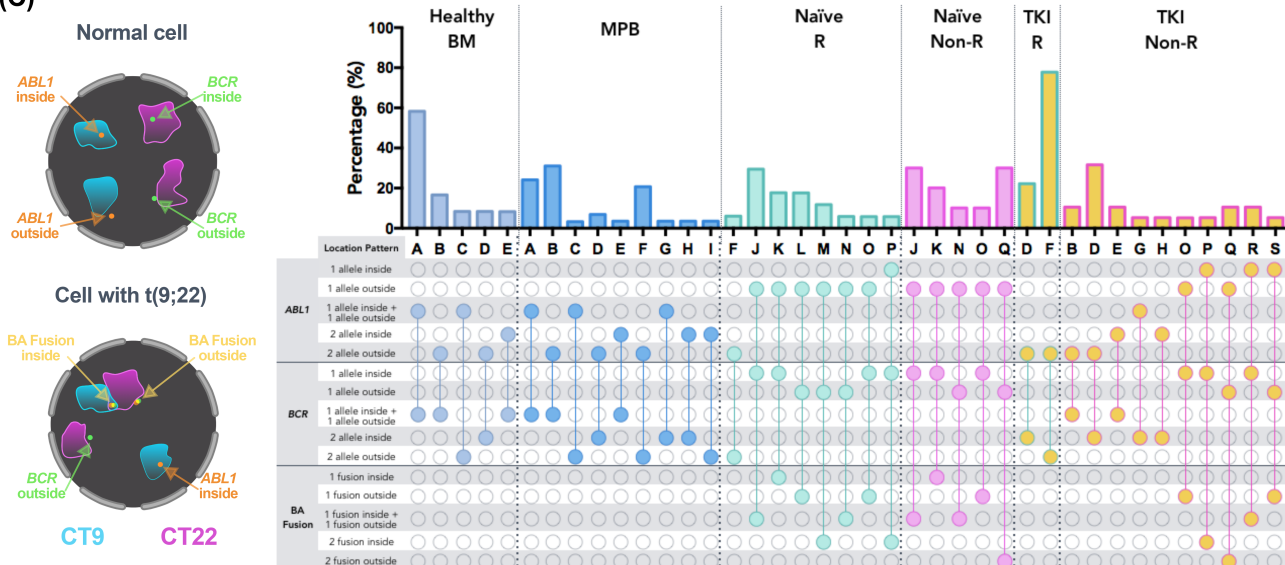


FIGURE 5 Genes relocate with reference to their CTs in the presence of t(9;22). (A) Three-dimensional reconstruction of the ABL1 (orange) and BCR (green) genes and their respective CTs, CT9 (cyan) and CT22 (magenta). Four probes were simultaneously hybridized to determine the distribution/position of the genes with reference to their respective CT (inside or outside). A representative 3D reconstruction per group is shown. (B) Three-dimensional reconstruction showing the z-projection of every cell appearing in A. ABL1 (orange) and BCR (green) and their respective CT, CT9 (cyan) and CT22 (magenta), probes were hybridized in the same test. (C) *Left*: Schematics showing the BCR and ABL1 allele locations (inside/outside) in reference to their respective CTs in a normal cell and in a cell with a BA fusion gene. *Right*: Upset plot showing the different location combinatorial patterns of the BCR and ABL1 alleles and the BA fusion gene with respect to CT9 and CT22 [Color figure can be viewed at wileyonlinelibrary.com]

CT22 in nonresponder groups. Given that the condensation of chromatin is characterized by a volume reduction due to a spatial organization into densely packed higher-order structures,³⁹ we qualitatively evaluated the CTs volumes using a condensation factor (CDF), which considers both the CT volume and the length of the DNA molecule corresponding to the chromosome.³¹ The significant increase of CTs decondensation, particularly in CT22, beyond being related to the

observed disruption patterns, could be associated with domain reorganization and, therefore, result in deregulation of the interchromosomal and intrachromosomal interactions. Differences in the interchromosomal interactions between CT9 and CT22 were evidenced by the increased intermingling volume in nonresponder groups. Furthermore, in agreement with previous studies,¹³ we found that less-condensed CTs exhibit a higher proportion of intermingling.

The physiological implications of these regions have been widely studied; and the degree of intermingling can be used as a qualitative measurement of the relative chromosomal positions, and it has been suggested that regions of chromosome intermingling potentially contain a higher density of regulatory sequences and could mediate interactions between chromosomes.⁴⁰ Interestingly, intermingling volumes correlate better with transcriptional activity than the distance between CT centroids,⁴¹ in which case our results suggest a proportional relationship between a smaller distance between CT9 and CT22 and a higher intermingling volume.

Notably, intermingling regions have been considered a factor promoting translocations,¹³ in line with the association between the proximity of sequences and their greater probability of translocation.⁴² Interestingly, the proportion of CD34+ cells with intermingling between the heterologous CT increases significantly in the TKI-R group in comparison to healthy controls, and also of interest, the level of intermingling in some of these cells is as high as the intermingling observed in cells with the t(9;22) translocation. Likewise, closer minimum distances between the *BCR* and *ABL1* genes are observed in the TKI-R in comparison to the healthy controls. Though enticing, further studies are necessary to understand the contribution of these topological features in the genesis and reappearance of t(9;22) when TKI-R CML patients stop treatment.

Considering that histone PTMs are inherently involved in the regulation and dynamics of chromatin condensation and preserve cell-type-specific chromosome organization,⁴³ we evaluated two histone marks representative of the open and closed chromatin states, H3K9ac and H3K27me3, respectively. Taken together, our results reveal a differential presence of histone PTMs not only between the responders and nonresponders CML groups but also between individual CTs in a single population. These observations are in line with the argument that the domain-wide differences in the enrichment of these modifications provide a global signature for each domain and CT within which more localized levels of functional control operate.⁴⁴ Nevertheless, chromatin structure is the result of an intricate and dynamic interplay between histone variants, PTMs, localization, histone chaperones and ATP-dependent nucleosome remodelers; thus, further studies are necessary to reveal the complete epigenetic landscape that regulates both the differential topological features between CTs and the deregulated mechanisms behind the CTs disruption.

We also searched for changes in the nuclear radial position of CTs among groups. Previous studies have indicated that CT positioning correlates with gene density^{45,46} and chromosome size.^{47,48} Consistent with these studies, we observed that in healthy hematopoietic cells CT9 localizes toward the nuclear periphery compared to CT22, and unexpectedly, we found that their positions were preserved in all groups, despite the presence of t(9;22). Maintenance of CT positioning is probably associated with the high content of pericentromeric heterochromatin in CT9 and the NOR regions in CT22, which could result in position stability.^{34,49} Nonetheless, the relative radial positions of the *BCR* and *ABL1* genes were not stable, and the position of the BA fusion significantly changed (even among the populations

carrying t(9;22)), this variability could respond to cell-specific transcriptional requirements. Additionally, the disrupted CT positions in non-R CML patients evidently changed the position parameters of the BA fusion, particularly in the TKI non-R group. Heterogeneity in the position of *BCR* and *ABL1* was also observed in relation to their respective CTs, and the presence of t(9;22) impacted the localization patterns of the BA fusion and the *BCR* and *ABL1* allelic pairs. It has been suggested that long-range chromatin decondensation (looping out) localizes active genes to the CT's edge or away from the CT-mediated transcriptional activity⁵⁰⁻⁵²; however, limited experimental data exist on this topic. Here, we show a panorama of major variability in the location patterns of *BCR*, *ABL1* and the BA fusion gene, if this structure is linked to any genome activity patterns it should be explored.

From another point of view, the CTs disruption and topological changes found in nonresponders CML patients leads us to reconsider the evolutionary processes happening during the carcinogenesis of this leukemia, which until now has been described as having an evolutionary pattern fitting with a stepwise microevolution phase.^{53,54} Although CML cells are considered to be highly homogenous due to the ubiquity of the Ph chromosome, our results suggest that more cellular heterogeneity than originally thought is present in this leukemia due to the large-scale 3D reorganization of the genome. In cancer evolutionary terms, the cellular heterogeneity conferred by this 3D reorganization could be another system of disease progression, probably by generation of new altered karyotypes and clones resistant to TKI. In fact, the presence of additional chromosomal aberrations increases during the evolution of CML, from 7% in early phases to 40% to 70% in advanced CML.⁵³ In addition, the positive response to Imatinib is near to 80% in the early stages of the disease, where almost no additional aberrations other than the Ph chromosome are evident, and falls drastically to nearly 8% during blast crisis, even when t(9;22) is present. In this context, the observed 3D genome reorganization might be due to the selection of preexisting and treatment-induced clones with chromosomal aberrations, the likely beginning of a cancer macroevolution cycle.⁵⁴ Further systematical studies are needed to address this approach.

Although the essays conducted in our study were limited by the number of cells and their irrecoverable nature, being BM a primary tissue of challenging access and restricted quantity, our results open new insights for the study of resistance to TKI treatment in CML. Some questions arising include: is the disruption of CTs 9 and 22 a phenomenon restricted only to the chromosomes involved in t(9;22)? Does disruption affect other CTs or is it a global phenomenon similar to genomic chaos? Given that CML progression implies the appearance of chromosomal alterations in addition to the Ph chromosome, how would the co-occurrence of these or other chromosomal alterations impact the nuclear topology of these cells? Could additional cryptic chromosomal aberrations be present in the analyzed cells that go overlooked due to resolution limitations inherent to the G-banding karyotype? In addition, and since the 3D genome organization affects transcriptional regulation, what cellular processes and regulatory mechanisms are affected in cells with highly disrupted CT9 and 22?

How does the epigenetic and transcriptome profile change in these cells? Comprehensive studies including super-resolution microscopy, chromosome capture methods and large-scale genome sequencing in single cells are required to solve these questions and determine their role in TKI resistance in CML.

Currently, the regulation and detailed mechanisms involved in genome compartmentalization, domain formation and determination of CTs positioning, are largely unknown (an extensive review on this field is available³). However, the functional consequences of disrupting the 3D genome can affect important cellular processes and eventually lead to disease and influence its progression.^{37,55,56} Our discovery proposes a model that can contribute to identifying genetic and epigenetic alterations that disrupt the 3D structure of the genome, mainly in cells of CML patients nonresponsive to treatment. Furthermore, our findings address the topological properties of CT9 and CT22, as well as the *BCR* and *ABL1* genes, in CML patients and provide a new overview of chromatin conformation that could be related to clinical prognosis. Additional studies will be critical to delineate the factors and mechanisms involved in chromatin disruption in CML patients who do not respond to TKIs, however, the ability to develop tools with the capacity to detect these cellular differences when CML patients arrive at the clinic for the first time would contribute significantly to their diagnosis, risk stratification, and potential treatments.

ACKNOWLEDGEMENTS

We want to thank all the patients and donors who participated in our study. We are thankful to the Hematology Department of INCAN for all the facilities provided during sample collection and patient care, particularly Dr Flavio A. Grimaldo and Dr Gilberto I. Barranco Lampón. We are grateful to the Blood Bank Department of INCAN, and specially to the members of the Cryobiology lab, Armando Juárez Nicolás, Alexia Andrade Mondaca, Beatriz Amanda Ochoa Robledo and Areli Eunice Hernández Alcántara, for their invaluable support obtaining MPB samples. We thank all the members of the laboratory of Dr Herrera at the Research Department of INCAN, for discussions and recommendations throughout the progress of the project.

CONFLICT OF INTEREST

The authors declare no conflict of interest.

AUTHOR CONTRIBUTIONS

Conceptualization: Eunice Fabian-Morales, Alfredo Rodríguez, Rodrigo González-Barrios and L.A.H.; Data curation: Eunice Fabian-Morales, Alfredo Rodríguez and Rodrigo González-Barrios; formal analysis: Eunice Fabian-Morales and Alfredo Rodríguez; Funding acquisition: Luis A. Herrera; Investigation: Eunice Fabian-Morales and Adriana Gudiño; Methodology: Eunice Fabian-Morales, Adriana Gudiño and Yameli L. Rodríguez Torres; Project administration: Eunice Fabian-Morales and Adriana Gudiño; Resources: Eunice Fabian-Morales, Adriana Gudiño, Yameli L. Rodríguez Torres, Clementina Castro Hernández, Alfredo H. de la Torre-Luján, Diego A. Oliva Rico and Alejandro López Saavedra; Software: Eunice Fabian-Morales, David

Vallejo-Escamilla and Erandhi C. Ornelas Guzmán; Supervision: Luis A. Herrera and Sara Frias; Validation: Eunice Fabian-Morales and Adriana Gudiño; Visualization: Eunice Fabian-Morales; Writing—original draft preparation: Eunice Fabian-Morales, Alfredo Rodríguez, Rodrigo González-Barrios and Sara Frias; Writing—review and editing, Eunice Fabian-Morales, Alfredo Rodríguez, Rodrigo González-Barrios, Sara Frias and Luis A. Herrera.

DATA AVAILABILITY STATEMENT

Images, data and further details are available from the authors upon request and with permission of the Instituto Nacional de Cancerología (INCan).

ETHICS STATEMENT

The study was conducted according to the guidelines of the Declaration of Helsinki and approved by the ethics and research committees of INCAN, México (authorization protocol 013/030/ICI CEI/856/13, approval 13 November 2013). Informed consent was obtained from all subjects involved in the study.

ORCID

Eunice Fabian-Morales  <https://orcid.org/0000-0002-3122-1055>
 Adriana Gudiño  <https://orcid.org/0000-0001-6925-2538>
 Alfredo Rodríguez  <https://orcid.org/0000-0002-1072-8631>
 Rodrigo González-Barrios  <https://orcid.org/0000-0001-8982-6586>
 Yameli L. Rodríguez Torres  <https://orcid.org/0000-0002-3793-6940>
 Clementina Castro Hernández  <https://orcid.org/0000-0002-5641-3627>
 Diego A. Oliva-Rico  <https://orcid.org/0000-0003-3115-3934>
 Erandhi C. Ornelas Guzmán  <https://orcid.org/0000-0001-8453-4533>
 Alejandro López Saavedra  <https://orcid.org/0000-0002-3838-4738>
 Sara Frias  <https://orcid.org/0000-0002-3097-6368>
 Luis A. Herrera  <https://orcid.org/0000-0003-3998-9306>

REFERENCES

1. Szabo Q, Bantignies F, Cavalli G. Principles of genome folding into topologically associating domains. *Sci Adv.* 2019;5:eaaw1668.
2. Lieberman-Aiden E, van Berkum NL, Williams L, et al. Comprehensive mapping of long-range interactions reveals folding principles of the human genome. *Science.* 2009;326:289-293.
3. Misteli T. The self-organizing genome: principles of genome architecture and function. *Cell.* 2020;183:28-45.
4. Wang S, Su J-H, Beliveau BJ, et al. Spatial organization of chromatin domains and compartments in single chromosomes. *Science.* 2016;353:598-602.
5. Cremer T, Cremer M. Chromosome territories. *Cold Spring Harb Perspect Biol.* 2010;2:a003889.
6. Kumaran RI, Thakar R, Spector DL. Chromatin dynamics and gene positioning. *Cell.* 2008;132:929-934.
7. Parada LA, McQueen PG, Misteli T. Tissue-specific spatial organization of genomes. *Genome Biol.* 2004;5:R44.
8. Schlesinger S, Meshorer E. Open chromatin, epigenetic plasticity, and nuclear organization in Pluripotency. *Dev Cell.* 2019;48:135-150.
9. Bonev B, Cavalli G. Organization and function of the 3D genome. *Nat Rev Genet.* 2016;17:661-678.

10. Bickmore WA, Teague P. Influences of chromosome size, gene density and nuclear position on the frequency of constitutional translocations in the human population. *Chromosome Res.* 2002;10:707-715.
11. Roukos V, Voss TC, Schmidt CK, Lee S, Wangsa D, Misteli T. Spatial dynamics of chromosome translocations in living cells. *Science.* 2013;341:660-664.
12. Sathitruangsak C, Righolt CH, Klewes L, Tung Chang D, Kotb R, Mai S. Distinct and shared three-dimensional chromosome organization patterns in lymphocytes, monoclonal gammopathy of undetermined significance and multiple myeloma. *Int J Cancer.* 2017;140:400-410.
13. Branco MR, Pombo A. Intermingling of chromosome territories in interphase suggests role in translocations and transcription-dependent associations. *PLoS Biol.* 2006;4:e138.
14. Kozubek S, Lukášová E, Marecková A, et al. The topological organization of chromosomes 9 and 22 in cell nuclei has a determinative role in the induction of t(9,22) translocations and in the pathogenesis of t(9,22) leukemias. *Chromosoma.* 1999;108:426-435.
15. Lukášová E, Kozubek S, Kozubek M, et al. Localisation and distance between ABL and BCR genes in interphase nuclei of bone marrow cells of control donors and patients with chronic myeloid leukaemia. *Hum Genet.* 1997;100:525-535.
16. Quintás-Cardama A, Cortes J. Molecular biology of bcr-abl1-positive chronic myeloid leukemia. *Blood.* 2009;113:1619-1630.
17. Hochhaus A, Baccarani M, Silver RT, et al. European LeukemiaNet 2020 recommendations for treating chronic myeloid leukemia. *Leukemia.* 2020;34:966-984.
18. García-Gutiérrez V, Hernández-Boluda JCC. Current treatment options for chronic myeloid leukemia patients failing second-generation tyrosine kinase inhibitors. *J Clin Med.* 2020;9:2251.
19. Bintu B, Mateo LJ, Su J-H, et al. Super-resolution chromatin tracing reveals domains and cooperative interactions in single cells. *Science.* 2018;362(6413).
20. Cremer M, Schmid VJ, Kraus F, et al. Initial high-resolution microscopic mapping of active and inactive regulatory sequences proves non-random 3D arrangements in chromatin domain clusters. *Epigenetics Chromatin.* 2017;10:39.
21. Deininger MW, Shah NP, Altman JK, et al. Chronic myeloid leukemia, version 2.2021, NCCN clinical practice guidelines in oncology. *J Natl Compr Canc Netw.* 2020;18:1385-1415.
22. Galinsky I, Buchanan S. Guide to interpreting disease responses in chronic myeloid leukemia. *J Adv Pract Oncol.* 2012;3:225-236.
23. Zhang WW, Cortes JE, Yao H, et al. Predictors of primary imatinib resistance in chronic myelogenous leukemia are distinct from those in secondary imatinib resistance. *J Clin Oncol.* 2009;27:3642-3649.
24. McGowan-Jordan J, Hastings R, Moore S. *ISCN 2020: An International System for Human Cytogenomic Nomenclature 2020.* Basel, Switzerland: Karger; 2020:145.
25. Dick JE. Stem cell concepts renew cancer research. *Blood.* 2008;112:4793-4807.
26. Fialkow PJ. Chronic myelocytic leukemia: origin of some lymphocytes from leukemic stem cells. *J Clin Invest.* 1978;62:815-823.
27. Solovei I, Cremer M. 3D-FISH on cultured cells combined with immunostaining. *Methods Mol Biol.* 2010;659:117-126.
28. Chaumeil J, Micsinai M, Skok JA. Combined immunofluorescence and DNA FISH on 3D-preserved interphase nuclei to study changes in 3D nuclear organization. *J Vis Exp.* 2013;72:e50087.
29. Demmerle J, Innocent C, North AJ, et al. Strategic and practical guidelines for successful structured illumination microscopy. *Nat Protoc.* 2017;12:988-1010.
30. Hook EB. Exclusion of chromosomal mosaicism: tables of 90%, 95% and 99% confidence limits and comments on use. *Am J Hum Genet.* 1977;29:94-97.
31. Wang Y, Nagarajan M, Uhler C, Shivashankar GV. Orientation and repositioning of chromosomes correlate with cell geometry-dependent gene expression. *MBoC.* 2017;28:1997-2009.
32. Bártošová E, Krejčí J, Harnicarová A, Galiová G, Kozubek S. Histone modifications and nuclear architecture: a review. *J Histochem Cytochem.* 2008;56:711-721.
33. Saksouk N, Simboeck E, Déjardin J. Constitutive heterochromatin formation and transcription in mammals. *Epigenetics Chromatin.* 2015;8:3.
34. van Steensel B, Belmont AS. Lamina-associated domains: links with chromosome architecture, heterochromatin, and gene repression. *Cell.* 2017;169:780-791.
35. Guelen L, Pagie L, Brasset E, et al. Domain organization of human chromosomes revealed by mapping of nuclear lamina interactions. *Nature.* 2008;453:948-951.
36. Ye CJ, Stilgenbauer L, Moy A, Liu G, Heng HH. What is karyotype coding and why is genomic topology important for cancer and evolution? *Front Genet.* 2019;10:1082.
37. Akdemir KC, Le VT, Chandran S, et al. Disruption of chromatin folding domains by somatic genomic rearrangements in human cancer. *Nat Genet.* 2020;52:294-305.
38. Zhou Y, Gerrard DL, Wang J, et al. Temporal dynamic reorganization of 3D chromatin architecture in hormone-induced breast cancer and endocrine resistance. *Nat Commun.* 2019;10:1522.
39. Mora-Bermúdez F, Ellenberg J. Measuring structural dynamics of chromosomes in living cells by fluorescence microscopy. *Methods.* 2007;41:158-167.
40. Uhler C, Shivashankar GV. Chromosome intermingling: mechanical hotspots for genome regulation. *Trends Cell Biol.* 2017;27:810-819.
41. Maharana S, Iyer KV, Jain N, Nagarajan M, Wang Y, Shivashankar GV. Chromosome intermingling—the physical basis of chromosome organization in differentiated cells. *Nucleic Acids Res.* 2016;44:5148-5160.
42. Meaburn KJ, Misteli T, Soutoglou E. Spatial genome organization in the formation of chromosomal translocations. *Semin Cancer Biol.* 2007;17:80-90.
43. Bannister AJ, Kouzarides T. Regulation of chromatin by histone modifications. *Cell Res.* 2011;21:381-395.
44. Wu R, Terry AV, Singh PB, Gilbert DM. Differential subnuclear localization and replication timing of histone H3 lysine 9 methylation states. *MBoC.* 2005;16:2872-2881.
45. Boyle S, Gilchrist S, Bridger JM, Mahy NL, Ellis JA, Bickmore WA. The spatial organization of human chromosomes within the nuclei of normal and emerin-mutant cells. *Hum Mol Genet.* 2001;10:211-219.
46. Tanabe H, Müller S, Neusser M, et al. Evolutionary conservation of chromosome territory arrangements in cell nuclei from higher primates. *Proc Natl Acad Sci USA.* 2002;99:4424-4429.
47. Bolzer A, Kreth G, Solovei I, et al. Three-dimensional maps of all chromosomes in human male fibroblast nuclei and prometaphase rosettes. *PLoS Biol.* 2005;3:e157.
48. Cremer M, von Hase J, Volm T, et al. Non-random radial higher-order chromatin arrangements in nuclei of diploid human cells. *Chromosome Res.* 2001;9:541-567.
49. Mangan H, Gailín MÓ, McStay B. Integrating the genomic architecture of human nucleolar organizer regions with the biophysical properties of nucleoli. *FEBS J.* 2017;284:3977-3985.
50. Nagano T, Lubling Y, Stevens TJ, et al. Single-cell hi-C reveals cell-to-cell variability in chromosome structure. *Nature.* 2013;502:59-64.
51. Paz N, Felipe-Blanco I, Royo F, et al. Expression of the DYRK1A gene correlates with its 3D positioning in the interphase nucleus of down syndrome cells. *Chromosome Res.* 2015;23:285-298.

52. Torabi K, Wangsa D, Ponsa I, et al. Transcription-dependent radial distribution of TCF7L2 regulated genes in chromosome territories. *Chromosoma*. 2017;126:655-667.
53. Horne SD, Stevens JB, Abdallah BY, et al. Why imatinib remains an exception of cancer research. *J Cell Physiol*. 2013;228:665-670.
54. Ye JC, Horne S, Zhang JZ, Jackson L, Heng HH. Therapy induced genome chaos: a novel mechanism of rapid cancer drug resistance. *Front Cell Dev Biol*. 2021;9:1432.
55. Agmon N, Liefshitz B, Zimmer C, Fabre E, Kupiec M. Effect of nuclear architecture on the efficiency of double-strand break repair. *Nat Cell Biol*. 2013;15:694-699.
56. Karakaidos P, Karagiannis D, Rampias T. Resolving DNA damage: epigenetic regulation of DNA repair. *Molecules*. 2020;25:2496.

SUPPORTING INFORMATION

Additional supporting information may be found in the online version of the article at the publisher's website.

How to cite this article: Fabian-Morales E, Vallejo-Escamilla D, Gudiño A, et al. Large-scale topological disruption of chromosome territories 9 and 22 is associated with nonresponse to treatment in CML. *Int. J. Cancer*. 2022;150(9):1455-1470. doi:10.1002/ijc.33903